Ultrasonically Enhanced Pre-leaching for the Removal of Organic Substances from Bauxite and Recovery of Leachate Through Wet Oxidation

Mengnan Li[1], Zhanwei Liu[2], Jiaping Zhao[3] and Wanzhang Yang[4]
1. Doctoral student
2. Professor
3, 4. Professor-level Senior Engineer
Kunming University of Science and Technology - Faculty of Metallurgical and Energy Engineering - National Engineering Research Center for Vacuum Metallurgy, Kunming, China
1. Doctoral student
2. Professor
Aluminium Industry Engineering Research Center of Yunnan Province, Kunming, China
Corresponding author: zhanwei_liu@126.com
https://doi.org/10.71659/icsoba2025-bx006

Abstract

Organic impurities in bauxite severely hinder the normal production of alumina. This study proposes a low-temperature ultrasonic-enhanced alkaline leaching process aimed at directly separating organic impurities from bauxite and purifying the leachate through H_2O_2 oxidation and CaO precipitation. Under optimal conditions of ultrasonic power at 550 W, temperature at 80 °C, time at 60 min, and NaOH concentration at 200 g/L, the leaching rate of organic carbon from bauxite reached 91.02 %, an improvement of 19.01 % compared to traditional leaching methods. XRD analysis of bauxite samples before and after leaching, along with results from XRF, carbon-sulphur analysis, SEM-EDS, and AFM, confirmed the effective separation of organic impurities without causing any loss of bauxite, with the alumina to silica ratio increasing to 34.13. Subsequently, 20 % H_2O_2 and 800 mL/g of CaO were added to the leachate. Under ultrasonic power of 550 W and oxidation at 90 °C for 60 min, the organic carbon removal rate was 71.35 %. GC-MS analysis confirmed the successful removal of major organic compounds from the leachate, while the XRD results of the oxidation residue indicated that organic compounds were ultimately removed in the form of $CaC_2O_4{\cdot}H_2O$ and $CaCO_3$. Furthermore, the study elucidated the radical reaction mechanism of H_2O_2 in oxidizing organic compounds in alkaline solutions. The proposed process operates at low temperatures and atmospheric pressure, generating no waste during the process, making it a clean, low-energy, and efficient method for the direct separation of organic substances from bauxite.

Keywords: Ultrasonic-enhanced leaching, Bauxite, Organic impurities, H_2O_2 oxidation, Clean processing.

1. Introduction

Alumina has been widely used in multiple fields such as ceramic manufacturing, electronics industry, catalyst preparation, construction materials, laser materials, and high-temperature materials due to its excellent properties and characteristics including low density, high melting point, high boiling point, strong corrosion resistance, and high hardness [1, 2]. Currently, on a global scale, the Bayer process, which utilizes bauxite as the raw material, remains the primary method for alumina production [3, 4]. However, due to the presence of a certain proportion of organic impurity in bauxite and the continuous accumulation of organic impurity during the Bayer liquor circulation process [5], the harm caused by organic impurity has long constrained the sustainable development of the alumina industry [6, 7].

Almost all the organic impurity in the Bayer process is introduced by bauxite, making the harm caused by organic impurity an inevitable issue [8]. In the dissolution process of bauxite, organic impurities will also dissolve in the sodium aluminate solution [9]. After the organic impurities dissolve in the sodium aluminate solution, they first alter the physical and chemical properties of the solution. One significant change is the increase in the dynamic viscosity of the sodium aluminate solution [10]. This not only makes the separation of red mud more difficult but also reduces the decomposition rate of seed, resulting in a decrease in the precipitation rate of aluminium hydroxide [11]. Secondly, the dissolved organic impurities form a layer of organic film on the surface of bauxite, which hinders the chemical mass transfer between the alkaline solution and the ore, directly reducing the leaching rate of alumina [12]. In addition, organic impurities can lead to a finer particle size and reduced strength of the resulting aluminium hydroxide products. This is detrimental to sedimentation and classification processes of aluminium hydroxide [13, 14]. Furthermore, organic impurities can decrease the whiteness of the final alumina product, resulting in lower product quality and impacting economic returns [15]. Lastly, the precipitation of low-molecular-weight oxalates can lead to accelerated scaling rates in decomposition tanks and reduce the lifespan of equipment [16, 17]. There is experimental data indicating that when the organic substance content in the Bayer liquor is 2.57 g/L, the seed decomposition rate decreases by 3.45 % [18]. In addition, for every 1 g/L increase in sodium oxalate concentration, the alumina output concentration will decrease by 1–2 g/L [19]. Therefore, it is essential to find a way to remove organic impurities from the Bayer process for the development of the alumina industry.

Currently, there are publicly reported methods for removing organic impurities from the Bayer process: bauxite roasting [20–22], mother liquor roasting [23], flotation [24, 25], crystallization [26], precipitation [27–29], ion exchange [30-32], membrane treatment [33,34], and wet oxidation [35, 36]. The above methods have their own advantages and limitations, which hinder their widespread adoption and implementation on a large scale. Compared to the enormous energy consumption generated by pyrometallurgical processes such as roasting, hydrometallurgy technology has more advantages.

In recent years, ultrasound has shown unique advantages as a novel intensification technology in the field of metallurgy [37]. Ultrasound is a type of mechanical wave with a frequency higher than 20 kHz, possessing high energy and short wavelength. During the wet leaching process, the cavitation and mechanical vibration effects generated by ultrasound can enhance the mass transfer of microbubbles formed in the liquid between the liquid and solid phases, and accelerates the movement of solid particles and uniformly disperses them in the solution [38]. When the microbubbles burst, not only does the solution's temperature temporarily increase, but microjets are also created at the solid-liquid interface. This reduces the thickness of the diffusion layer at the solid-liquid interface through stripping and erosion, generates new reaction interfaces, and accelerates the leaching reaction rate [39]. Compared to conventional leaching, ultrasound-enhanced leaching has the advantages of improved leaching effect and shortened leaching time, thereby reducing the apparent activation energy of the reaction and decreasing energy consumption [40].

In conclusion, this study utilized low-temperature ultrasonic-enhanced alkaline leaching to directly separate organic impurity from bauxite, and completed a closed-loop process by purifying the leaching solution through H_2O_2 wet oxidation and CaO precipitation. The effects of different experimental parameters (ultrasonic power, temperature, time and NaOH concentration) on the leaching rate of total organic carbon (TOC) were investigated. Furthermore, H_2O_2 oxidation and CaO precipitation technology were employed to oxidize and precipitate organic substances in leaching solutions to achieve the goal of recovering the leaching solution. The study also discussed the reaction mechanism of H_2O_2 oxidizing organic substance in alkaline solution.

2. Materials and Methods

2.1 Materials

The material used in this experiment was bauxite provided by an alumina factory in Yunnan Province, China. After the raw ore was retrieved, it was processed by crushing, grinding, ore screening, and other processes, and the -80 mesh (< 0.177 mm approx..) was dried for 10 hours as material. The analytical grade pure sodium hydroxide, calcium oxide, and hydrogen peroxide used in the experiment were sourced from Tianjin Feng Chuan Chemical Reagent Co., Ltd.

2.2 Experimental Equipment and Methods

The equipment used in this study is a heatable ultrasonic generator, manufactured by Shanghai Shengxi Ultrasonic Instrument Co., Ltd. The ultrasonic power ranges from 0 to 550 W, the ultrasonic frequency is 40 kHz, the heating power is 2000 W, and the temperature control range is from room temperature to 99 °C.

As shown in Figure 1, the bauxite and a certain concentration of NaOH solution are mixed in a 500 mL PTFE beaker according to a certain liquid-solid ratio (L/S) and put into the ultrasonic generator that has been preheated to the set temperature, and leaching for a specific duration. The present study investigated the impact of various leaching conditions on the leaching rate of TOC in bauxite. Then, H_2O_2 and CaO were mixed with the leaching solution in a PTFE beaker with a certain proportion and put into the ultrasonic generator that has been preheated to the set temperature and oxidized for a specific duration. The organic substance in the leaching solution is removed.

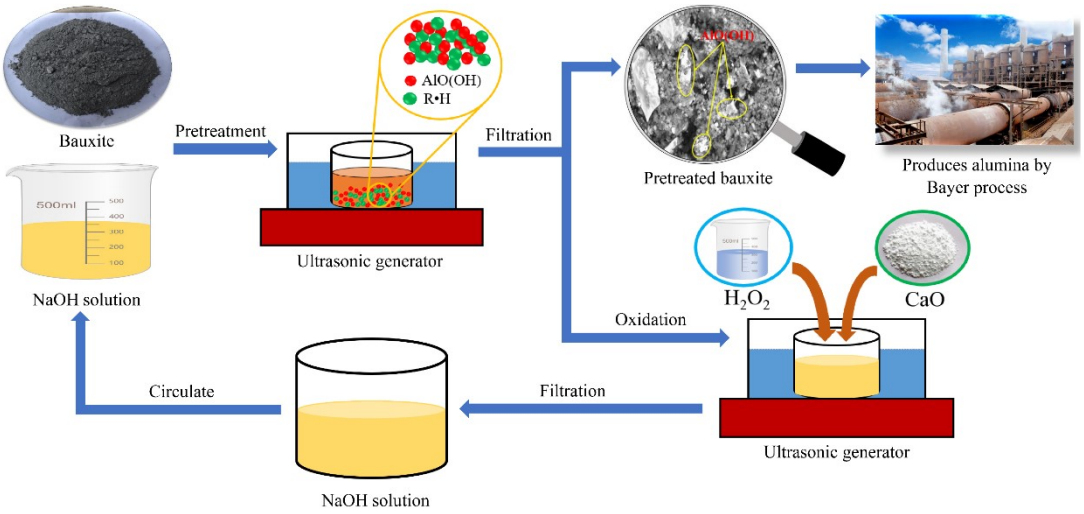

Figure 1. Schematic diagram of the process in this study.

2.3 Detection of TOC

In a 500 mL conical flask, 2 mL of the obtained filtrate, 100 mL of deionized water, and 10 mL of 20 % sulphuric acid solution are sequentially added. Then the liquid preparation is boiled and titrated while hot with 0.01 mol/L $KMnO_4$ solution until a pale pink colour is achieved and remains unchanged for 30 s. The volume of $KMnO_4$ solution added is recorded as V_a.
The next step consists in adding to the preparation, after its cooling down to room temperature, sequentially 10 mL of 0.01 mol/L $KMnO_4$ solution and 5 mL of sulphuric acid-silver sulphate solution. The new liquid preparation is boiled for 10 min, then 10 mL of 0.01 mol/L $Na_2C_2O_4$

solution is added meanwhile the boiling continues. While hot, the preparation is titrated with 0.01 mol/L $KMnO_4$ solution until a pale pink colour is achieved and remains stable for 30 s. The new added volume of $KMnO_4$ solution is recorded as V_b.
The concentration of TOC in the solution is calculated using Equation (1).

$$C_{TOC} = \frac{C_{KMnO_4} \times (V_a + V_b)}{2} \times \frac{5}{2} \times \frac{24}{134} \quad (1)$$

where:
C_{TOC} concentration of TOC, g/L
C_{KMnO4} concentration of $KMnO_4$, 0.01 mol/L

The formula for calculating the TOC leaching rate is shown in Equation (2).

$$\varphi = \frac{V \times C}{M_C} \quad (2)$$

where:
φ TOC leaching rate, %
V volume of the obtained leaching solution, L
C TOC content of the leaching solution, g/L
M_C TOC content in bauxite, g

Equation (3) was used to calculate the removal rate of TOC in the leaching solution.

$$\eta = (1 - \frac{V_2 \times C_2}{V_1 \times C_1}) \times 100\ \% \quad (3)$$

where:
η removal rate of TOC, %
V 2000 mL
V_2 volume of the filtrate after filtering the oxidized slag, (mL
C_1 TOC content in the leaching solution, g/L
C_2 TOC content in the solution after oxidation, g/L

3. Results and Discussion

3.1 Mineralogical Study of Organic Substances

The XRD and XRF analysis results of bauxite are shown in Figure 2 and Table 1, respectively, with the carbon content measured by the carbon/sulphur analyser. Figure 2 shows that the main mineral phases of the bauxite are diaspore (AlO(OH)), pyrite (FeS_2), anatase (TiO_2), hematite (Fe_2O_3), kaolinite ($Al_2Si_2O_5(OH)_4$), and Pyrophyllite ($Al_2Si_4O_{10}(OH)_2$). From Table 1, it can be observed that the total carbon (TC) and TOC contents of 0.69 and 0.59 %, respectively. The alumina to silica ratio (A/S) of the bauxite is 9.91. To obtain a more detailed understanding of the existence state of the carbon element, Figure 3 presents the results of SEM-EDS analysis of the material. In all the following EDS images, the presence of the Cu element is solely due to the background (in order to avoid the influence of conductive adhesive on the C element, copper foil was uniformly used for sample preparation).

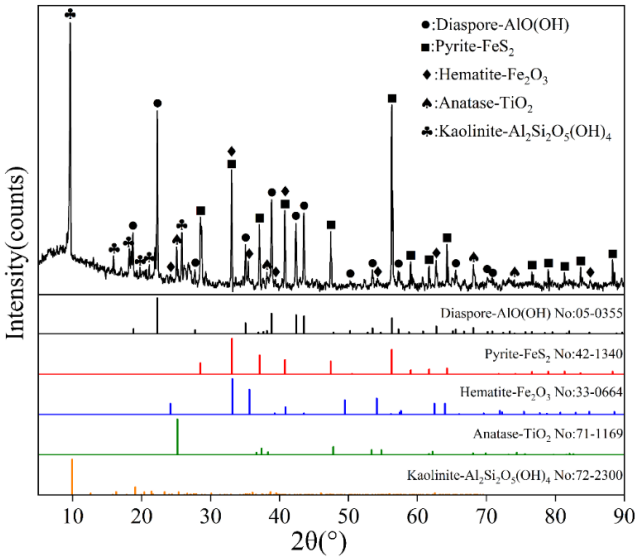

Figure 2. XRD analysis results of bauxite.

Table 1. Chemical composition analysis of bauxite.

Component	Al_2O_3	Fe_2O_3	SiO_2	TiO_2	CaO	C_T	C_{Toc}
Content (wt.%)	34.10	23.03	3.44	1.10	0.04	0.69	0.59

Figure 3a illustrates that the material consisted of particles of varying sizes. Although the various elements are unevenly distributed in the material, the mineral particles of diaspore, pyrite, and silicon minerals can be determined from the distribution areas and overlapping conditions of different elements. Furthermore, the surface of diaspore particles is relatively smooth, while the surfaces of pyrite and silicate mineral particles are rough, as shown in the Figure 3d. The distribution of carbon element is relatively dispersed, and no obvious mineral structure has been formed. Figure 3b displays the results of EDS analysis for the region shown in Figure 3a. It can be observed that the carbon element content is significantly higher than that detected by the carbon/sulphur analyser, indicating that carbon element is mainly distributed on the surface of the mineral. Therefore, during the element surface scan, the content of carbon element is relatively high.

The EDS spectra of points 1, 2, and 3 in Figure 3e are shown in Figs. 3f, g, and h, respectively. Points 1 and 2 are located in areas on diaspore, where the carbon element content is lower than the level that in Figure 3b. Due to the relatively smooth surface, the adsorption of organic substance on its surface is poor, resulting in a lower carbon element content. On the other hand, point 3 is in an area on a pyrite where the carbon element content is significantly higher than that in Figure 3b. Because of its relatively rough surface, the adsorption of organic substance on its surface is stronger, leading to a higher carbon element content.

By examining the chemical bonding patterns between carbon atoms and between carbon atoms and other atoms, it is possible to ascertain the predominant presence of organic carbon within the material. Figure 4 illustrates the findings. The X-ray photoelectron spectroscopy (XPS) spectrum in Figure 4a shows a full element scan. In Figure 4b, the high-resolution C 1s XPS spectra validate the existence of two primary bonding states of carbon atoms in the material: C=C (at approximately 283.6 eV) and C-C (at around 284.6 eV) bonds. Notably, the peak corresponding to the C=C bond displays the highest peak area, suggesting that the carbon element predominantly occurs in the form of organic carbon bonding in the material. Additionally, Figure 4c-f display the bonding configurations of the other four main atoms in the material, aligning with findings from XRD and SEM-EDS analyses.

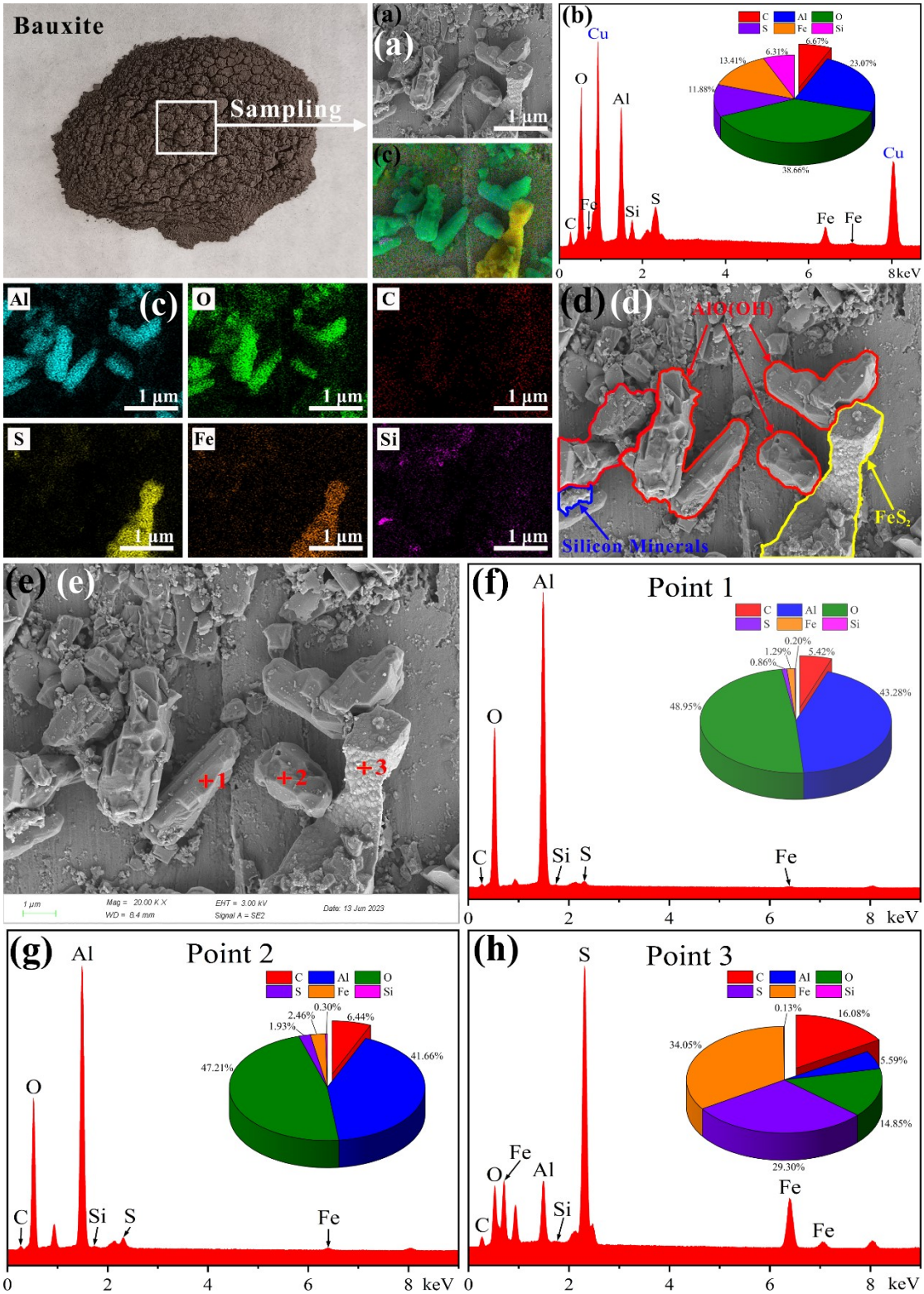

Figure 3. The SEM image (a), elemental surface scan (b), elemental mapping (c), main mineral markers (d), SEM image magnification (e), and EDS spectra of points 1 (f), 2 (g), and 3 (h) of the material.

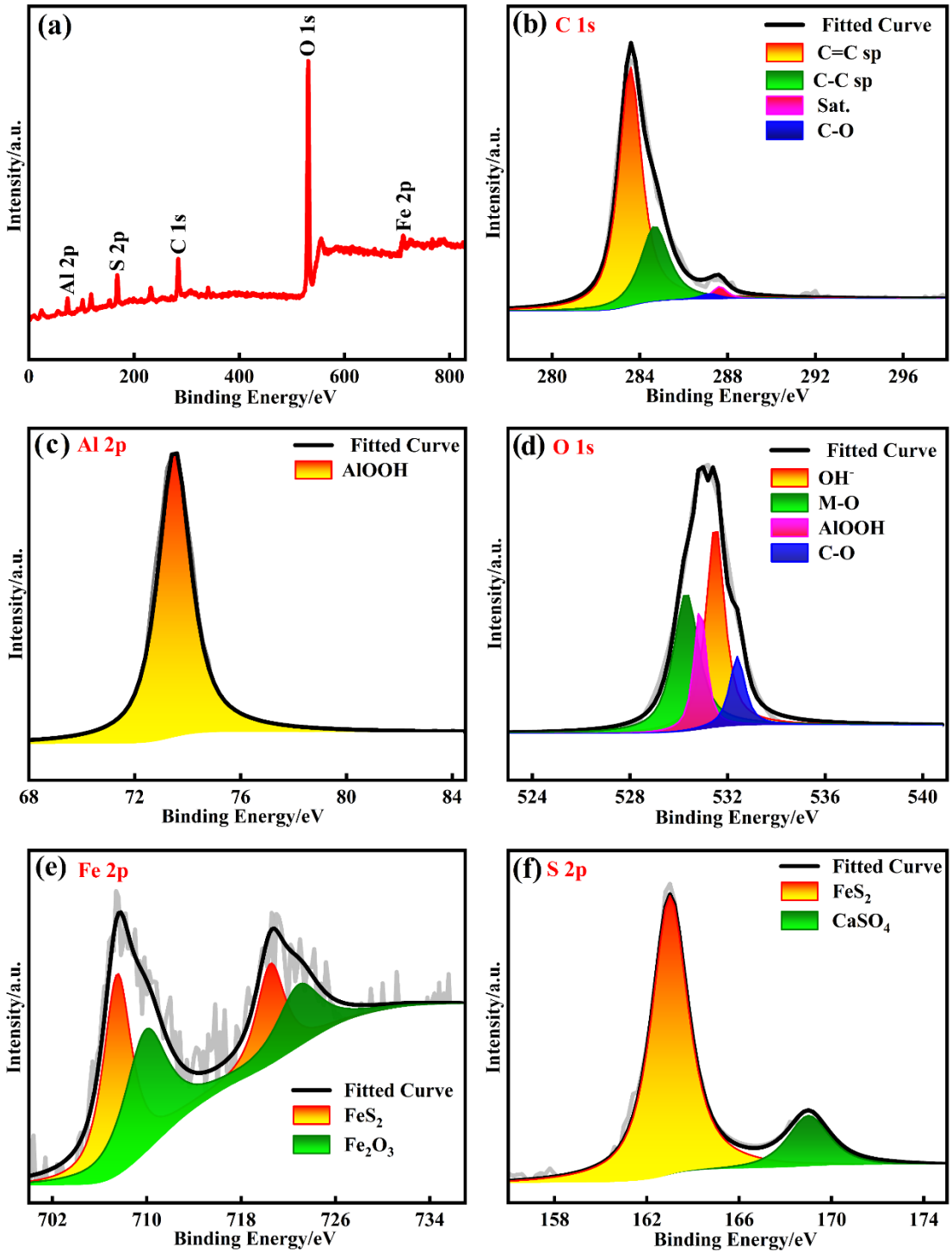

Figure 4. The XPS survey results of material.

According to the aforementioned mineralogical study of organic substances, it has been found that organic substances do not form mineral structures within bauxite. Instead, they adhere to the surface of bauxite, particularly concentrating on the surfaces of iron minerals and silicon minerals.

3.2 Effects of different factors on the leaching rate of TOC

3.2.1 Effect of ultrasonic power

Ultrasonic is a novel hydrometallurgy strengthening technique. The cavitation effect and mechanical vibration effect generated by ultrasonic waves are the essence of its ability to strengthen leaching processes. The cavitation effect refers to the dynamic process of growth and collapse that occurs when microbubbles in a liquid vibrate under the action of sound waves, at a certain sound pressure level. It is the primary way of energy transfer between ultrasound and liquids. The mechanical vibration effect can accelerate the collision between the leaching solution and the ore, continuously corroding the mineral surface by the leaching solution. Under the conditions of leaching temperature of 80 °C, L/S of 10 mL/g, and NaOH concentration of 200 g/L, the effect of ultrasonic power (0-550 W) on the leaching rate of TOC was studied, and the results are shown in Figure 5.

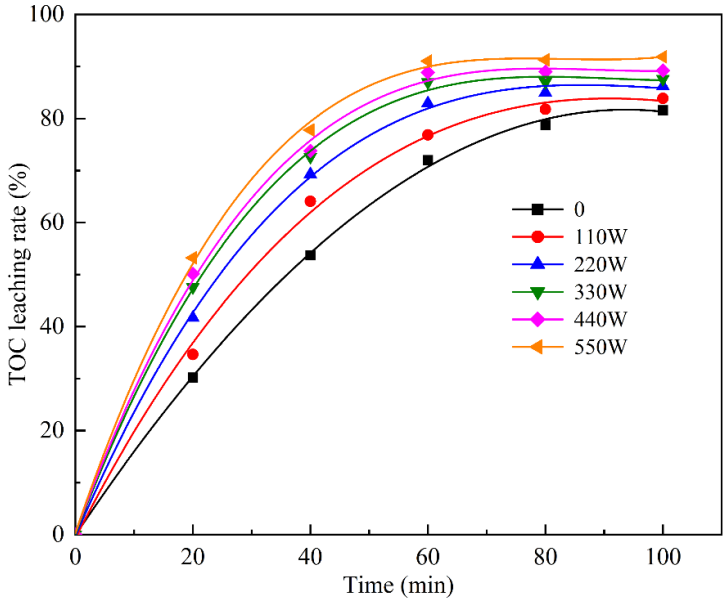

Figure 5. The variation of TOC leaching rate with time under different ultrasonic power.

From Figure 5, it can be seen that after ultrasonic-enhanced leaching, the leaching rate of TOC is significantly higher than that of conventional leaching (ultrasonic power equal to 0). Furthermore, compared to conventional leaching, the efficiency of ultrasonic-enhanced leaching is also higher. The leaching rate of TOC of 60 min of ultrasonic-enhanced leaching at 220 W has exceeded the leaching rate of TOC of 100 min of conventional leaching. The reason is that, as clarified in Section 3.1, organic substances are mainly attached to the surface of bauxite, without forming a mineral structure. Under the cavitation effect and mechanical vibration effect of ultrasound, the chemical mass transfer between the alkaline solution molecules and organic substances is accelerated, and the detachment of organic substances attached to the surface of bauxite is promoted. Based on the experimental results, a 550W ultrasonic power was ultimately chosen for subsequent research.

3.2.2 Effect of leaching temperature

Figure 6 shows that increasing the temperature can significantly improve the leaching rate of TOC. However, after surpassing 80 °C, further elevating the temperature resulted in little to no change in the leaching rate of TOC. The organic impurities in bauxite mostly exist in the form of humus, with a small portion present in the form of asphalt. Asphalt does not dissolve in the Bayer

process and will be discharged with red mud. However, humus is highly soluble in alkaline solutions, where they transform into various sodium organic acids present in sodium aluminate solutions, as shown in Table 4. The increase in temperature promotes the dissolution of humus, leading to an increase in the leaching rate of TOC, as shown in the Equation (4). In the equation, $R•H_n$ represents organic substance. After reaching a temperature of 80 °C, the dissolution reaction of organic substances in the solution reaches equilibrium, leading to a relatively stable leaching rate of TOC after 80 °C. So, 80 °C was selected as the optimal leaching temperature.

$$R•H_n + nNaOH \rightarrow R•Na_n + nH_2O \quad (4)$$

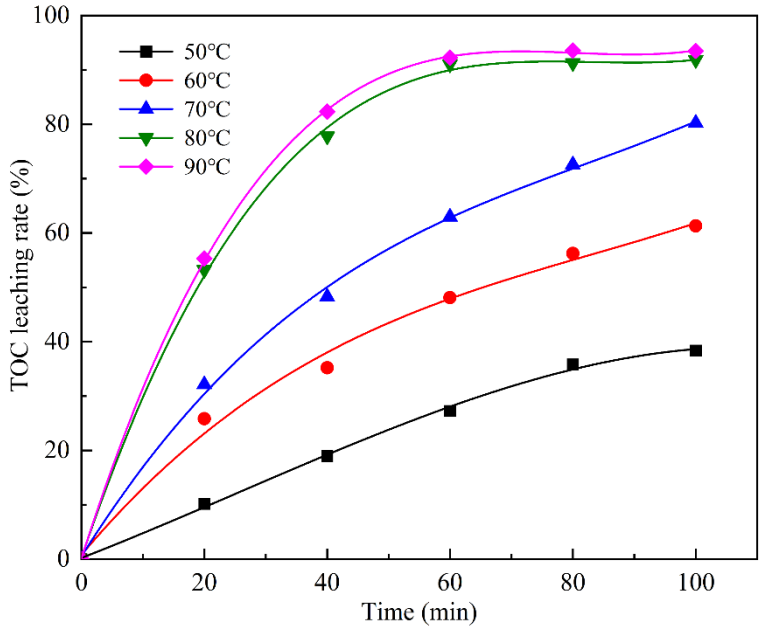

Figure 6. The variation of TOC leaching rate with time under different leaching temperature.

3.2.3 Effect of NaOH concentration

As shown in Figure 7, increasing the NaOH concentration significantly enhances the leaching rate of TOC. When the NaOH concentration is 0 g/L (equal volumes of deionized water), the maximum leaching rate of TOC is only 6.12 % as time progresses. However, when the NaOH concentration is raised to 50 g/L, the TOC leaching rate rapidly increases, reaching a plateau after the NaOH concentration is raised to 200 g/L. This is because the organic impurities in bauxite are mainly soluble humus, formed through a series of complex processes involving the decomposition of animal and plant debris under the action of the environment and microorganisms. While these substances are insoluble in water and acidic solutions, they dissolve in hot alkaline solutions. Therefore, increasing the NaOH concentration has a significant promoting effect on the leaching of TOC in bauxite, but this effect is limited. Consequently, when the NaOH concentration exceeds 200 g/L, the leaching rate of TOC shows minimal variation. Additionally, under conditions of 60 min and NaOH concentration of 200 g/L, the loss rate of alumina was only 1.21 %. This is because the temperature of 80 °C is insufficient to reach the temperature required for the leaching of diaspore, even with an NaOH concentration of 200 g/L. Thus, considering various factors, the optimal NaOH concentration of 200 g/L was selected.

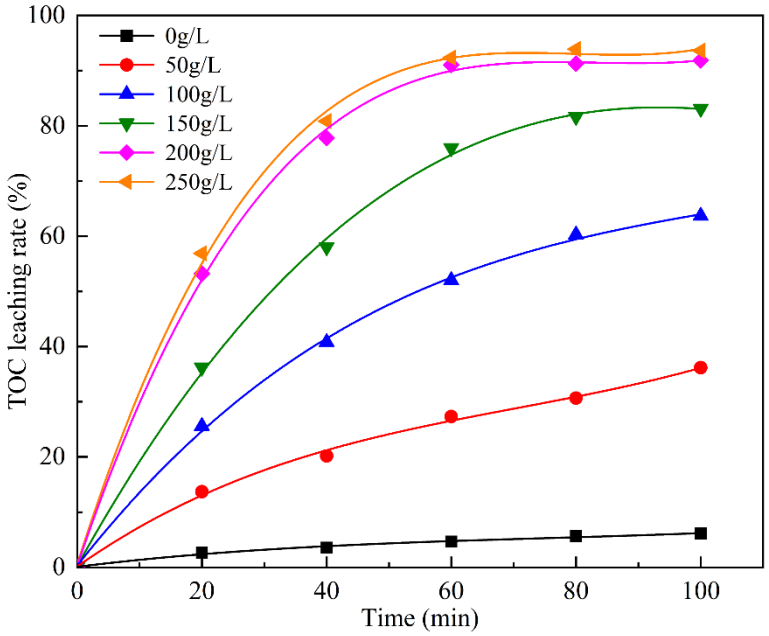

Figure 7. The variation of TOC leaching rate with time under different NaOH concentration.

3.3 Leaching kinetic research

Studying the kinetics of the leaching process can help identify the controlling steps, which is crucial for enhancing the leaching rate. The leaching of organic carbon from the surface of bauxite is a heterogeneous solid-liquid phase reaction. In this study, the organic carbon content was relatively low, and SEM-EDS analysis of the material shows that the organic substance does not form mineralized tissue but rather adheres to the surface of the bauxite. The main composition and particle size of the ore remain unchanged before and after leaching. Therefore, kinetic studies can benefit from the application of the shrinking core model. According to the theory of the shrinking core model, the reaction rate is influenced by two factors: the chemical reaction rate at the interface between the material and the product (chemical reaction control) and the diffusion rate of the liquid phase in the product layer (diffusion control). The kinetic equations are shown as Equations (5) and (6) [41, 42].

Chemical reaction control:

$$1-(1-x)^{1/3}=kt \tag{5}$$

Diffusion control:

$$1-\frac{2}{3}x-(1-x)^{2/3}=kt \tag{6}$$

where:

x leaching rate of organic carbon, %
k reaction rate
t leaching time, min

The Arrhenius equation is used to determine the activation energy of a reaction, as demonstrated in Equations (7) and (8).

$$k = A\, e^{-\frac{E_a}{RT}} \tag{7}$$

$$\ln k = -\frac{E_a}{RT} + \ln A \quad (8)$$

where:
A pre-exponential factor
E_a activation energy, J/mol
R ideal gas constant, 8.314 J/mol·K
T leaching temperature, K.
Equation (8) presents the logarithmic form of Equation (7).

Based on the experimentally obtained organic carbon leaching rates at different temperatures, linear fitting results for chemical reaction control and diffusion control were graphed as presented in Figures 8a and 8b based on the kinetic equations. The results reveal that both models exhibit high regression coefficients (R^2). The Arrhenius plots for the two control models are displayed in Figures 8d and 8e. The activation energy for the chemical reaction control model was calculated to be 34.26 kJ/mol, whereas for the diffusion control model, it was determined to be 59.33 kJ/mol.

In the leaching kinetics of solid-liquid heterogeneous reactions, the activation energy controlled by chemical reaction typically exceeds 40 kJ/mol, while the activation energy for reactions controlled by diffusion usually ranges between 8−20 kJ/mol. Additionally, Figures 8a and 8b indicate that the chemical reaction control model exhibits a better regression coefficient. Thus, based on the regression coefficients and activation energy values of the control models at various temperatures, this study concludes that the ultrasonically enhanced leaching of organic substance on bauxite surfaces is concurrently governed by chemical reactions and diffusion, and the activation energy is 34.26 kJ/mol.

From the variation of organic carbon leaching rate with time at different leaching temperatures in Figure 6, it can be observed that at temperatures below 70 °C, the increase in organic carbon leaching rate with temperature remains basically consistent at the same time, and the leaching rate of organic carbon continues to rise steadily with prolonged time, still increasing up to 100 min. This is a typical phenomenon of a diffusion control leaching process, as the leaching proceeds slowly and relatively consistent in rate under diffusion control. When the temperature is increased from 70 °C to 80 °C, the increase in organic carbon leaching rate at the same time is significantly greater than at temperatures below 70 °C. Furthermore, compared to temperatures below 70 °C, the leaching reaction of organic carbon is essentially completed by 60 min at 80 °C. This is a typical phenomenon of a leaching controlled by chemical reaction, as reactions proceed rapidly the rate of change is significant under chemical reaction control. This also indicates that the ultrasonic-enhanced leaching process of organic carbon in this study is jointly controlled by chemical reaction and diffusion.

3.4 Analysis of bauxite after leaching

The bauxite obtained under the optimal conditions of conventional leaching (leaching temperature 80 °C, leaching time 80 min, NaOH concentration 200 g/L, without ultrasonic enhancement) and ultrasonic-enhanced leaching (leaching temperature 80 °C, leaching time 60 min, NaOH concentration 200 g/L, ultrasonic power 550 W) were analysed by XRD, XRF, carbon/sulphur analyser, SEM-EDS, and Atomic Force Microscope (AFM). The obtained results were compared with the various analysis results of the original bauxite.

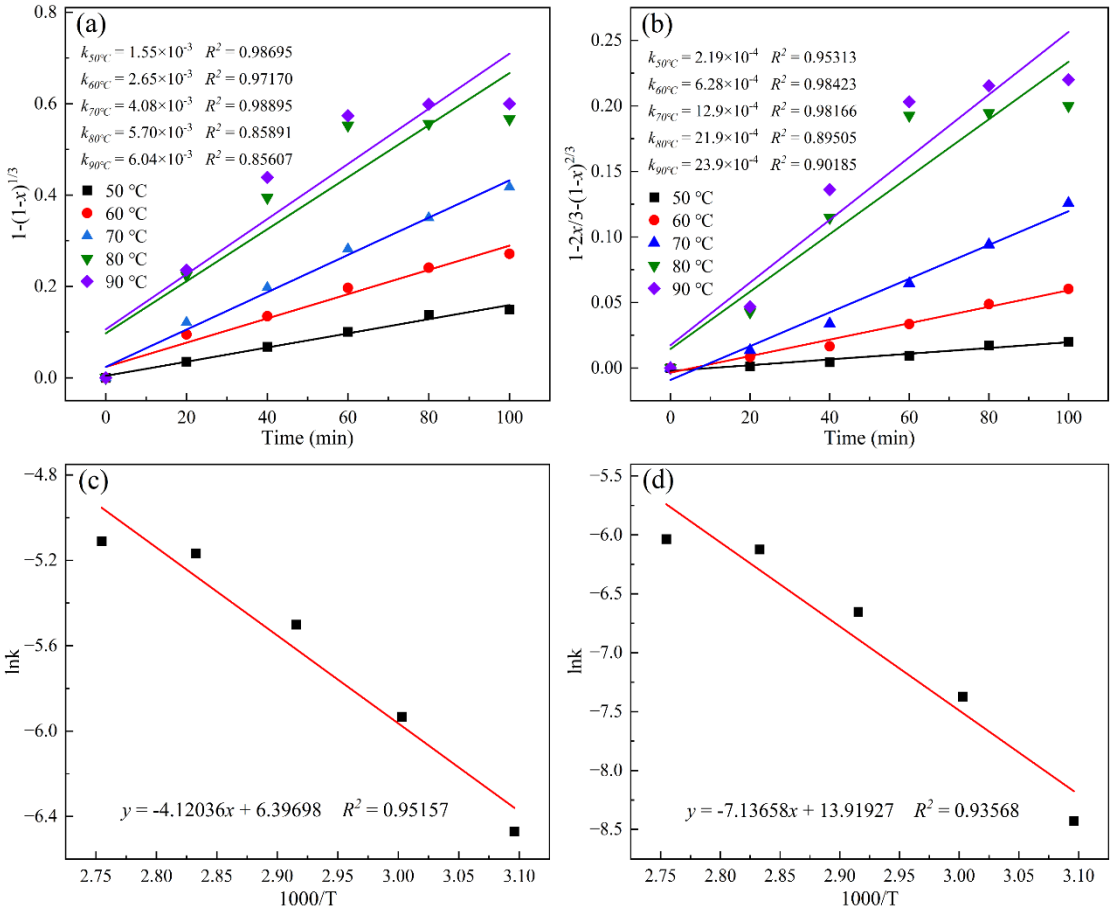

Figure 8. The fitting curve of chemical reaction control (a) and ln*k* -1000/*T* (c); The fitting curve of diffusion control (b) and ln*k* -1000/*T* (d).

3.4.1 XRD, XRF and carbon/sulphur analyser analysis

Figure 9 shows the comparison of XRD patterns of original bauxite, after conventional leaching and ultrasonic-enhanced leaching. It can be observed that the diffraction peaks of diaspore remain largely unchanged before and after leaching, but the diffraction peak of kaolinite at 2θ value of 9.92 degrees disappears significantly. By comparing the main chemical composition content of the samples in Table 2 with Table 1, it can be seen that after leaching, the content of Al_2O_3 is enriched, the content of SiO_2 is significantly reduced, and from the results of carbon and sulphur analyser, it is evident that the C_{TOC} content decreases significantly. Furthermore, the percentage of Al_2O_3 content in bauxite after ultrasonic-enhanced leaching is higher than that after conventional leaching, while the percentages of C_{TOC} and SiO_2 content are lower. These results demonstrate that low-temperature alkaline ultrasonic-enhanced leaching can effectively separate organic substance in bauxite without losing alumina, reducing silica content. Ultrasonic-enhanced leaching of bauxite not only removed 91.02 % of organic carbon but also increased the A/S of the bauxite to 34.13, which is very beneficial for the subsequent Bayer leaching process.

Table 2. Chemical composition of bauxite after leaching.

Component (wt.%)	Al_2O_3	Fe_2O_3	SiO_2	TiO_2	CaO	C_{Toc}
Conventional leaching	34.89	27.21	1.57	1.41	0.08	0.11
Ultrasonic-enhanced leaching	39.25	29.75	1.15	0.87	0.05	0.06

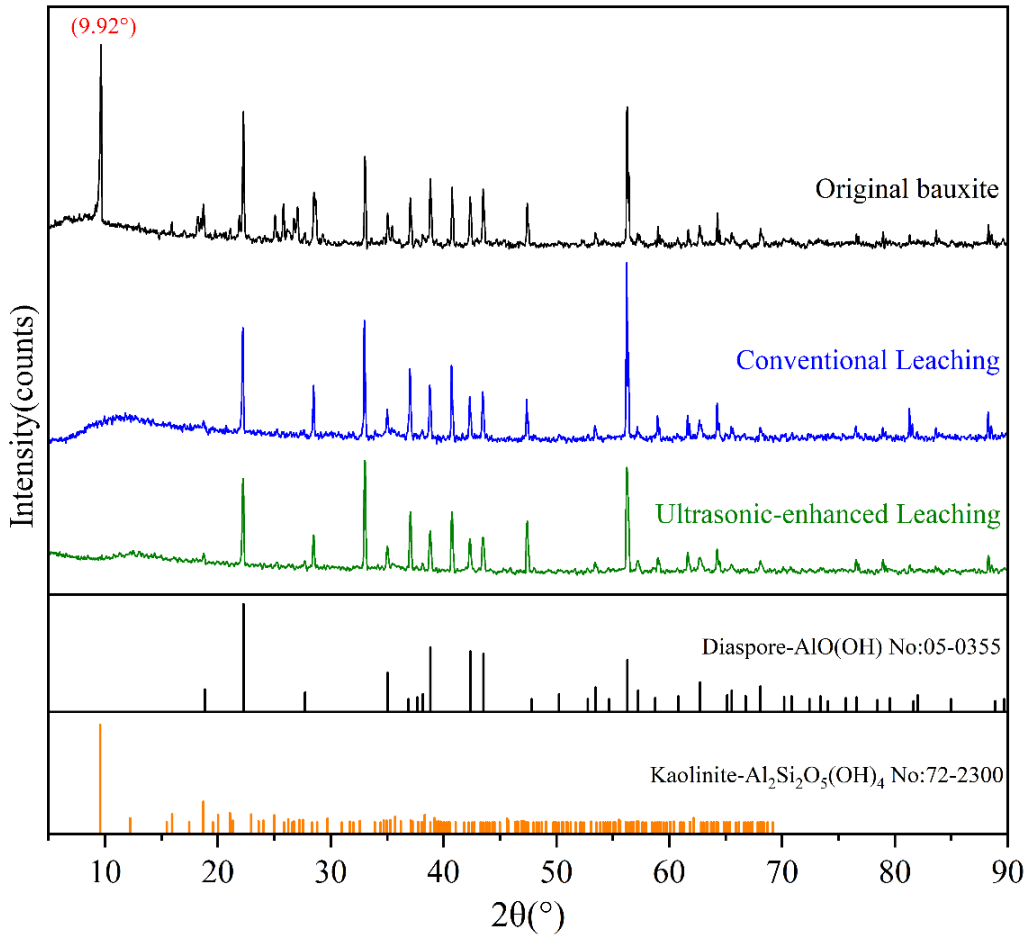

Figure 9. XRD analysis results of original bauxite, after conventional leaching and ultrasonic-enhanced leaching.

3.4.2 SEM-EDS analysis

By comparing Figure 10 and Figure 3, it is evident that before leaching, the distribution of carbon elements in bauxite is relatively extensive and dense. However, after conventional leaching treatment, the distribution area of carbon elements narrows, and the density decreases accordingly, indicating the removal of organic substance. EDS results from the overall area and three different positions all show a significant decrease in carbon element content compared to the original bauxite (Figures 10b, 10f, 10g and 10h). Compared to Figure 10, Figure 11 indicates that after ultrasonic-enhanced leaching treatment, the carbon element content is further reduced, and carbon elements are hardly found in the SEM area. EDS results also confirm that after ultrasonic-enhanced leaching treatment, only trace amounts of carbon elements are present in the bauxite. Importantly, intact diaspore particles can be observed, confirming that the process of this study effectively separates organic substance from bauxite while preserving intact diaspore particles.

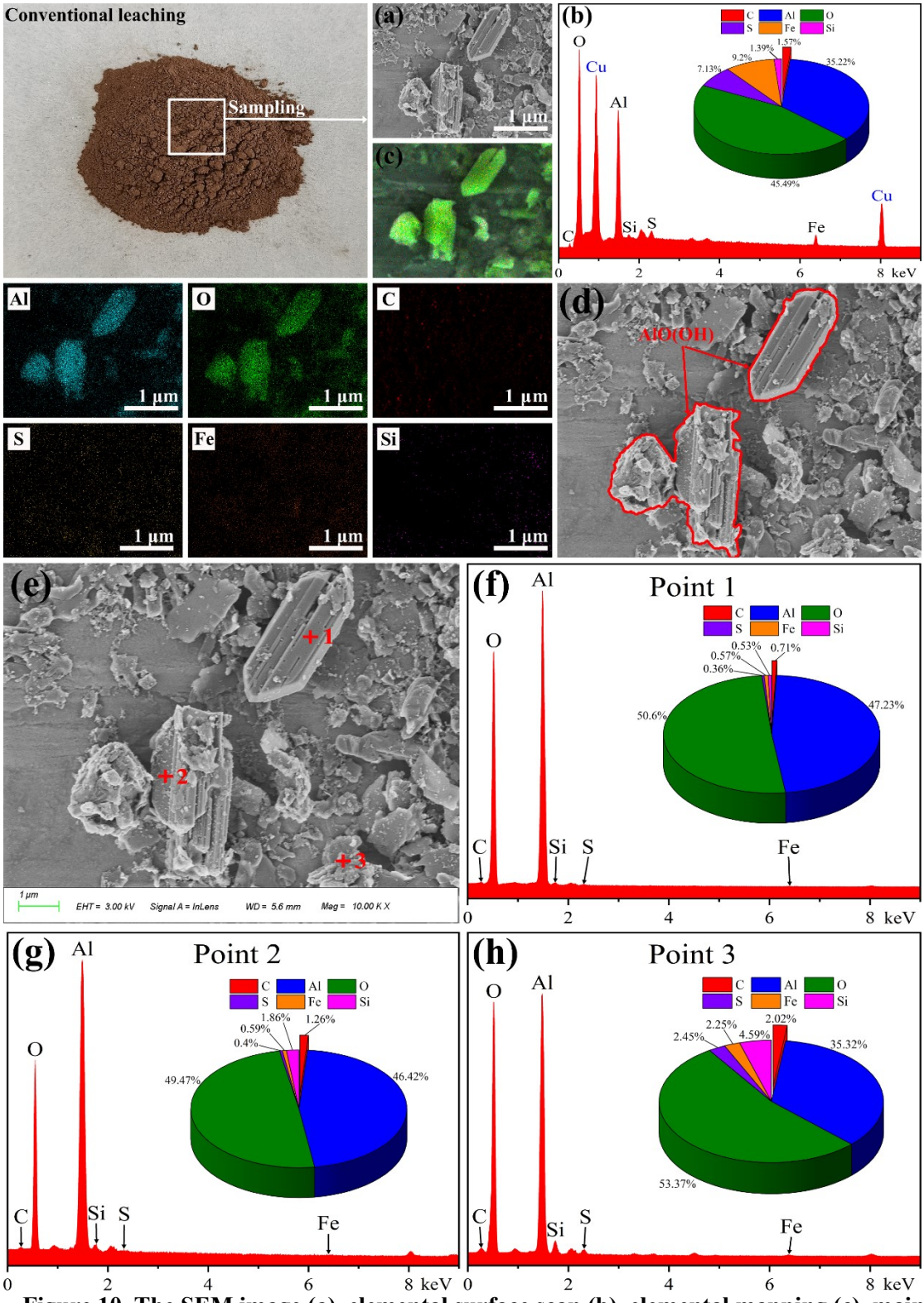

Figure 10. The SEM image (a), elemental surface scan (b), elemental mapping (c), main mineral markers (d), SEM image magnification (e), and EDS spectra of points 1 (f), 2 (g), and 3 (h) of the bauxite after conventional leaching.

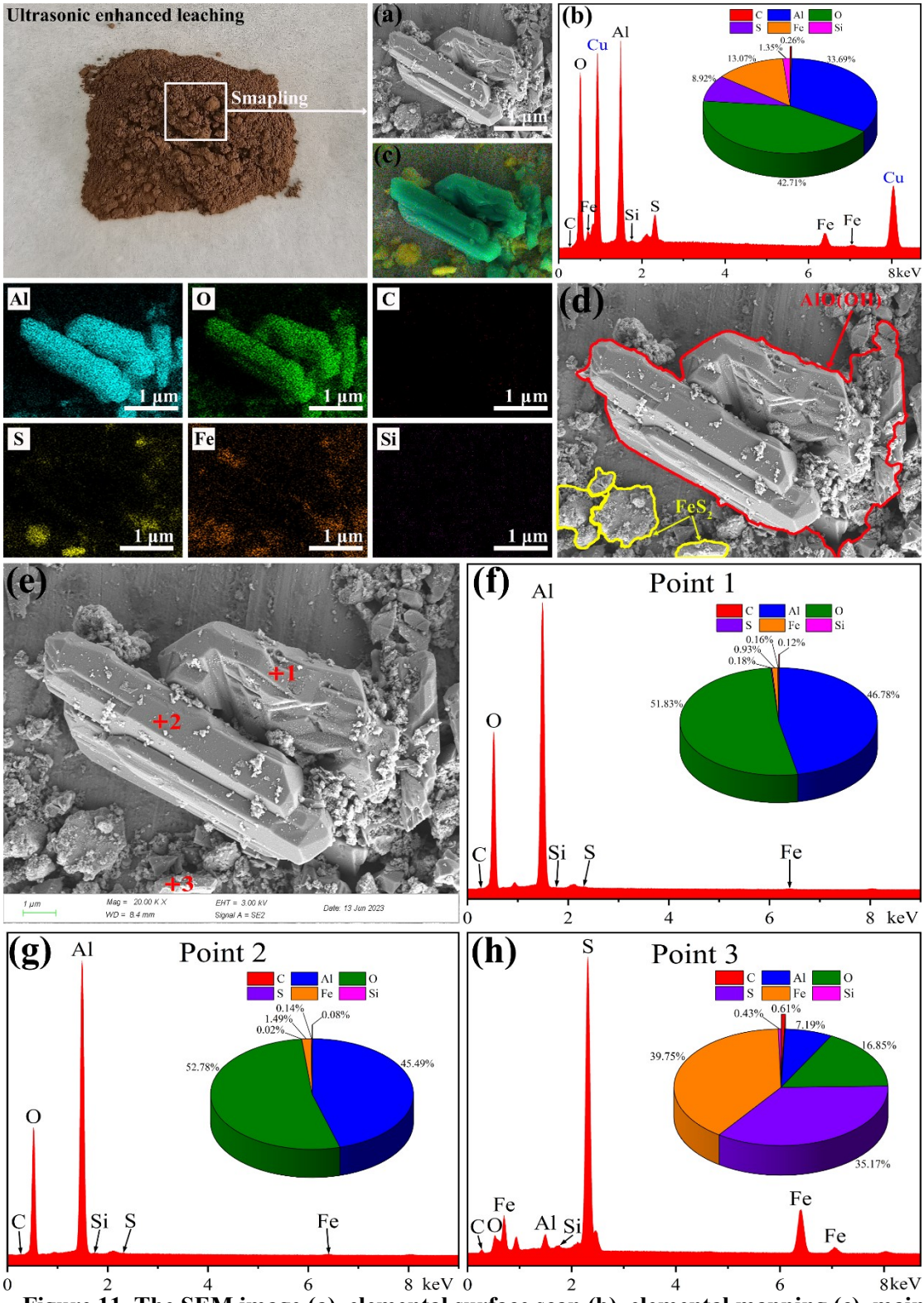

Figure 11. The SEM image (a), elemental surface scan (b), elemental mapping (c), main mineral markers (d), SEM image magnification (e), and EDS spectra of points 1 (f), 2 (g), and 3 (h) of the bauxite after ultrasonic-enhanced leaching.

3.4.3 AFM analysis

The AFM was used to detect the two-dimensional (2D) and three-dimensional (3D) surface height morphology features of different samples. The NanoScope Analysis 3.00 software was used to analyse the height probability cumulative distribution curve of the AFM images. The results are shown in Figure 12. The surface roughness of the samples can reflect the degree of erosion of NaOH solution on the sample surface. The average surface roughness and root mean square roughness of different samples are shown in Table 3.

The 3D height morphology images of different samples (scanning range of 2 × 2 μm) and height probability distribution curves show that, under the same height scale of 0–12 nm, the heights of peaks on the original bauxite surface are relatively uniform with small height differences (Figure 12a_2). 90 % of the peak heights are below 9.24 nm (H_{90} = 9.24 nm), and there are no peaks with heights exceeding 12 nm (Figure 12a_3). After conventional leaching, the height differences of peaks on the bauxite surface increase (Figure 12b_2), with peak heights concentrated between 9.86–10.79 nm (as shown in Figure 12b_3, H_{10} = 9.86 nm, H_{90} = 10.79 nm). After ultrasonic-enhanced leaching, the height differences of peaks on the bauxite surface further increase (Figure 12c_2), with a large number of peaks exceeding 12 nm. More than 50 % of the peaks have heights exceeding 11.82 nm, and more than 10 % of the peaks exceed 12.13 nm (Figure 12c_3).

The study in Section 3.1 has shown that organic substance does not form mineral structures in bauxite, but instead adsorbs on the surface of the bauxite, such as humic substances. So, the peaks on the sample surface are mainly mineral structures (such as diaspore, pyrite, hematite, etc.), with organic substance either adsorbed on the surface of these peaks, or filling the valleys between peaks, or accumulated on the mineral surface, forming some peaks. Therefore, as seen in Figure 12, the peak distribution on the surface of the original bauxite is the most within the same scanning range. Moreover, Table 3 shows that the surface roughness value of the original bauxite is the smallest, at Rq = 0.605 nm, because organic substance filling in the valleys between peaks would raise the original datum plane height of the mineral surface, making the peaks shorter. Organic substance adsorbed on the peak surface or forming peaks would make the mineral surface smoother, reducing surface roughness. After conventional leaching, NaOH reacts with organic substance, causing individually formed organic substance peaks to dissolve, reducing the number of peaks on the bauxite surface. Organic substance adsorbed on the peaks is stripped off, making the peaks slimmer. Organic substance filling in the valleys between peaks reacts with NaOH, lowering the mineral surface datum plane height, causing the peaks to become taller, and increasing surface roughness. All of these are confirmed by Figs. 12b_2 and 12b_3, and Table 3, showing that the number of prominent peaks on the surface of bauxite decreases, becomes higher, and the surface roughness increases (Rq = 0.675 nm) after conventional leaching.

The cavitation effect and mechanical vibration effect of ultrasound enhance the etching action of NaOH solution on the bauxite surface, strengthening the reaction between NaOH and organic substance. After ultrasound-enhanced leaching, within the same scanning range, there are fewer peaks on the bauxite surface, they are taller, and the surface roughness is further increased (Rq=1.290 nm), but the main peaks formed by minerals still exist (as shown in Figures 12c_2 and 12c_3, and Table 3). This indicates that ultrasound-enhanced leaching of bauxite effectively achieves the separation of organic substance without leaching out alumina.

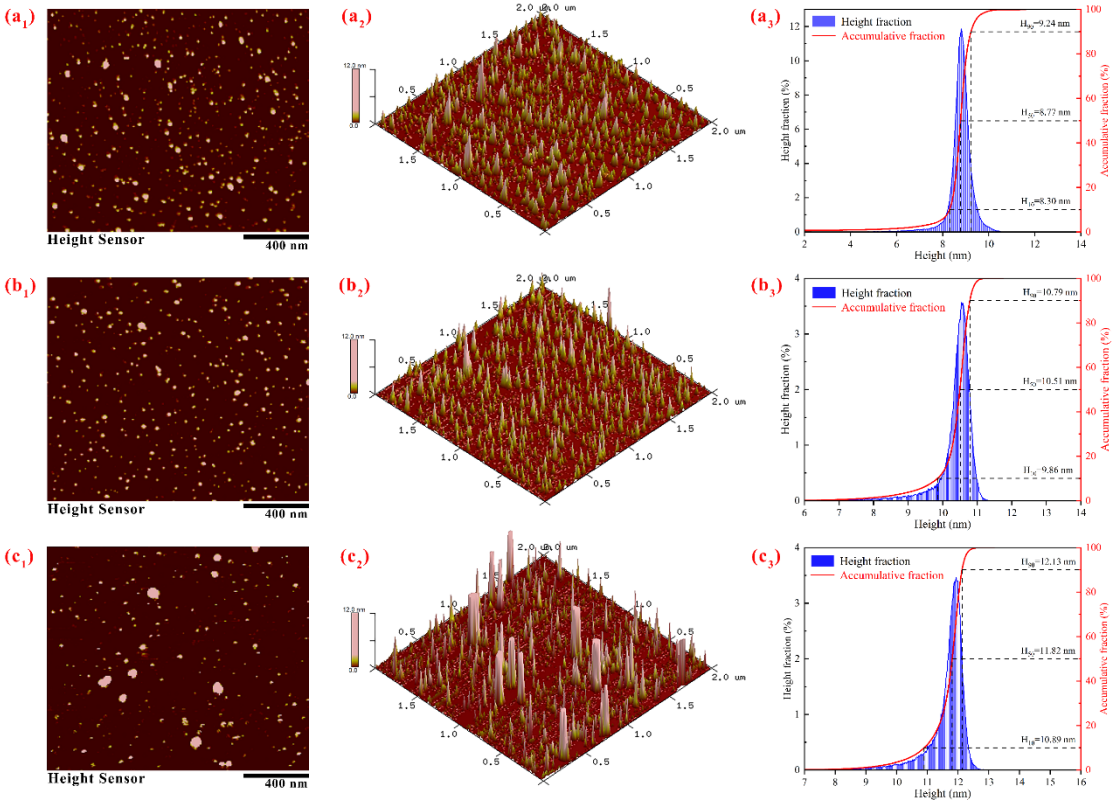

Figure 12. The AFM 2D and 3D surface height morphology features and height probability distribution curves of the original bauxite (a_1, a_2, and a_3), after conventional leaching (b_1, b_2, and b_3), and after ultrasonic-enhanced leaching (c_1, c_2, and c_3).

Table 3. Surface roughness of different samples (nm).

Surface roughness	Sample		
	Original bauxite	Conventional leaching	Ultrasonic-enhanced leaching
Rq	0.605	0.675	1.290
Ra	0.353	0.432	0.448

3.5 GC-MS analysis of the leaching solution

The original solution obtained from the experiment was first subjected to derivatization with saturated n-butanol, followed by esterification using 50 % hydrochloric acid. Finally, the esterification liquid was dehydrated using anhydrous magnesium sulphate to obtain the test solution. The test solution was filtered through a 0.22 μm microporous membrane filter and directly subjected to GC-MS analysis. The instrument model is 7890A-5975C gas chromatography-mass spectrometry (GC-MS) system, manufactured by Agilent Technologies, Inc. The results are shown in Figure 13.

From Figure 13, it can be seen that the types of organic substances and the relative abundance of major organic substances in the ultrasound-enhanced leachate are greater than those in conventional leachate, which once again confirms the advancement of ultrasound-enhanced leaching.

The peaks and residence times in Figure 13 were compared with the standard peaks in the database. The formed organic acids include 2-methylpropanoic acid, butanoic acid, stearic acid, formic acid, trans-butenedioic acid (fumaric acid), oxalic acid (ethanedioic acid), benzoic acid,

hexanoic acid, succinic acid (butanedioic acid), glutaric acid, 2-butenedioic acid, heptanedioic acid, hexadecanoic acid, dodecanoic acid, tridecanoic acid, octanedioic acid, nonanedioic acid, hexanedioic acid, octadecadienoic acid. The organic acids with higher contents in terms of relative content from high to low are: butanedioic acid, trans-butenedioic acid, butanoic acid, stearic acid, benzoic acid, oxalic acid, hexadecanoic acid, glutaric acid, dodecanoic acid. Alkane substances include: 2,3-dimethylpentane, 3,4-dimethylhexane, ethylene oxide, 2-methylpropane, dimethylisobutoxysilane, 1,1-diisobutoxyisobutane, 2-methylpropane, butane, 1,1-dibutoxybutane, n-octadecane, 2,2-dimethyleicosane, 1,1-dimethylethyl cyclohexane, 1,1,3-trimethyl cyclopentane, with the higher content of alkane being: dimethylisobutoxysilane, 1,1-diisobutoxyisobutane, 2-methylpropane, 3,4-dimethylhexane, 2,2-Dimethyleicosane. Other organic substances include but are not limited to: butene, benzene, acetone, formaldehyde, phenol, and ketone, but overall, the content of these types of organic substances is very low.

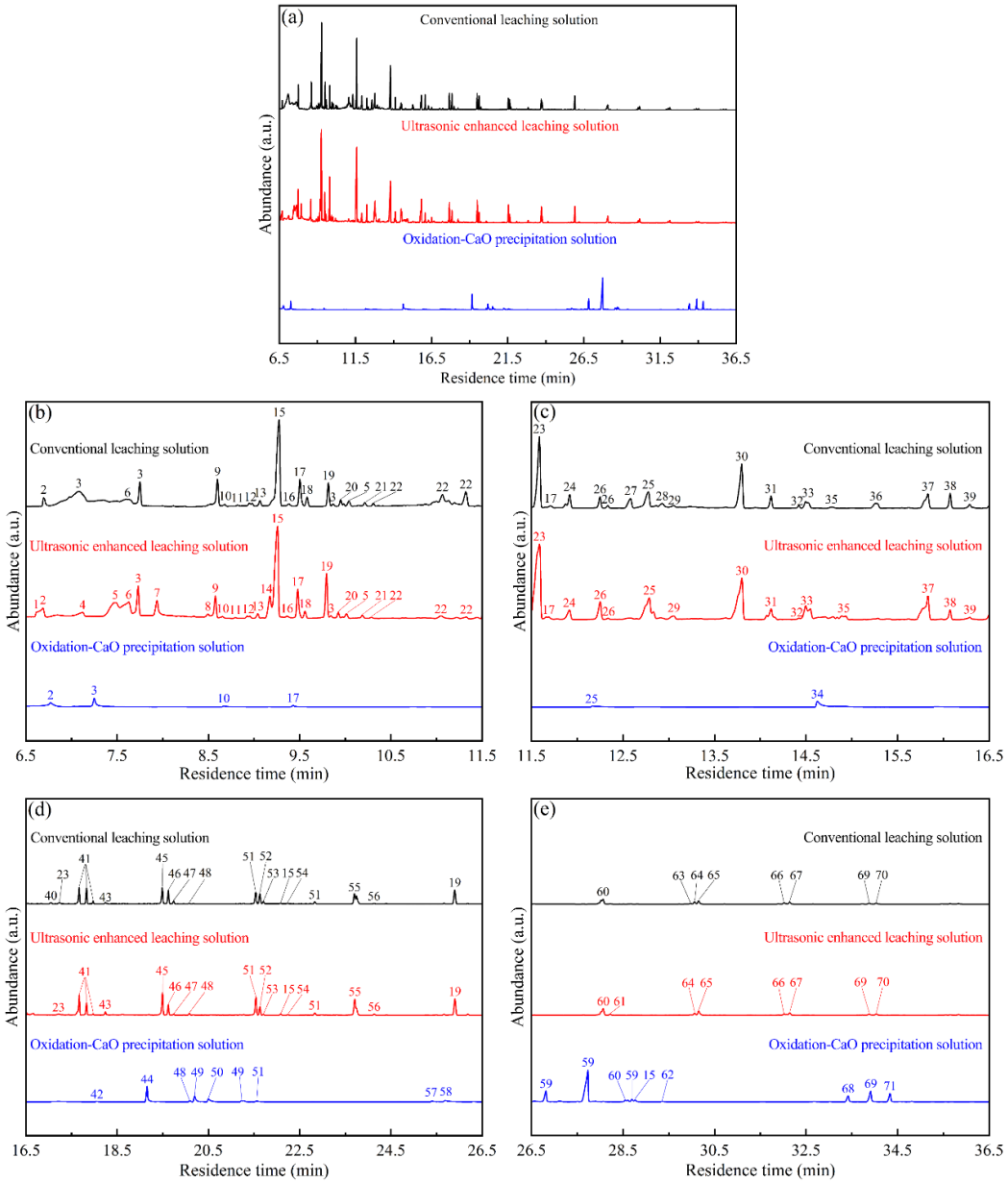

Figure 13. Total ion chromatography (a) and local magnification (b), (c), (d), (e) of the esterification solution of the conventional leaching solution, ultrasound-enhanced leaching solution, and H_2O_2 oxidation-CaO precipitation solution.

3.6 The H_2O_2 oxidation-CaO precipitation of the leaching solution

The methodology is the following:
Take the ultrasound-enhanced leaching solution obtained under the optimal condition of 2000 mL and place it in a PTFE beaker. H_2O_2 and CaO should be added at 20 % and 800 mL/g, respectively. Then put the beaker into the ultrasonic generator that was heated to 90 °C in advance, and oxidize it for 60 min under stirring conditions. After filtration, the TOC concentration in the oxidation solution was determined to be 0.16 g/L, whereas in the leaching solution it was 0.56 g/L. The calculated TOC removal rate of 71.35 %, obtained using Equation (3). Furthermore, Figure 13 shows that after treatment with H_2O_2 and CaO, most of the organic acids and alkanes in the leaching solution can be oxidized and removed, with residual organic substances mainly consisting of benzene derivatives.

During the degradation process of organic substances, a single reactant can generate multiple intermediate products throughout the oxidation process. The reaction mechanism of these intermediate products is also quite complex. In the solution, the oxidation mechanism of polymeric organic substances involves the transfer of electrons from the polymer to the oxidizing agent. This transfer leads to the formation of reactive free radicals or ions, which then react with other molecules in the solution. These reactions result in the cleavage of chemical bonds within the polymer, leading to the degradation of the polymer chains. In addition, the oxidizing agent can directly react with the polymer, causing further degradation of the organic substance. Overall, the oxidation mechanism of polymeric organic substances in solution involves complex interactions of electron transfer and free radical reactions [43].

In the process of organic substance degradation by H_2O_2 oxidation, H_2O_2 easily decomposes into HO_2^- (Eq. (9)), which promotes the decomposition of H_2O_2 to form hydroperoxyl radicals ($HO_2\cdot$) and hydroxyl radicals ($HO\cdot$) (Equation (10)). $HO_2\cdot$ further decomposes to form superoxide anion radicals ($O_2^-\cdot$) (Equation (11)). The hydroxyl radical ($\cdot OH$) can be regarded as the neutral form of the hydroxide ion (OH^-) with one electron lost, and it possesses an extremely strong oxidative capacity (oxidation-reduction potential of 2.8 V). It is the second strongest oxidant in nature after fluorine (oxidation-reduction potential of 3.05 V). The products of superoxide radicals are all powerful oxidants that can oxidize unsaturated fatty acids in lipids to form lipid peroxides. The effectiveness of H_2O_2 in removing organic substances is primarily determined by the combined action of the generated $HO_2\cdot$ intermediate and $HO\cdot$.

$$H_2O_2 \rightarrow H^+ + HO_2^- \quad (9)$$

$$H_2O_2 + HO_2^- \rightarrow HO_2^{\bullet} + HO\cdot + HO^- \quad (10)$$

$$HO_2^{\bullet} \rightarrow O_2^-\cdot + H^+ \quad (11)$$

Taking the oxidation of $Na_2C_2O_4$, which poses great harm in the Bayer liquor, as an example, the total reaction equation for its oxidation is shown in Equation (12). According to the calculations using HSC 6.0 software, within the temperature range of 0 to 100 °C, the standard Gibbs free energy of Equation (12) was determined to be negative, as illustrated in Figure 14. This suggests that Equation (12) is thermodynamically feasible. Moreover, the standard Gibbs free energy decreases with increasing temperature, indicating that higher temperatures favour the oxidation of organic substances.

$$H_2O_2 + Na_2C_2O_4 + 2NaOH \rightarrow 2Na_2CO_3 + 2H_2O \quad (12)$$

The specific oxidation process of $C_2O_4^{2-}$ is illustrated in Figure 15. One COO- group of $C_2O_4^{2-}$ is

activated by HO·, resulting in the formation of the activated intermediate I. Intermediate I reacts with O_2^{-}· generated by HO_2·, leading to the formation of the peroxide radical intermediate II. Intermediate II undergoes further activation to generate active intermediate III. This last is further activated by HO·, producing unstable species IV (peroxycarbonyl) and V (superoxide). IV decomposes to form stable CO_3^{2-} and H_2O, while V continues to react with HO· to generate stable CO_3^{2-} and H_2O. Based on the above conclusion, it can be inferred that the concentrations of HO· and O_2^{-}· in the system determine the rate of the oxidation reaction.

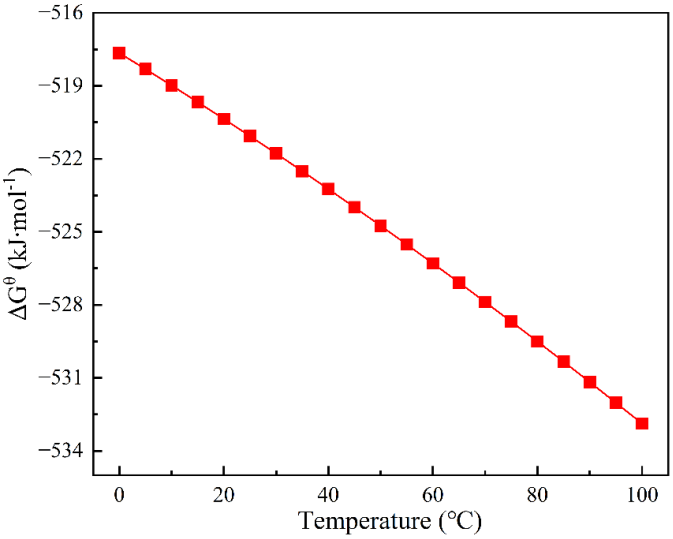

Figure 14. The ΔG^{θ} of the reaction in Eq. 8 at 0–100 °C.

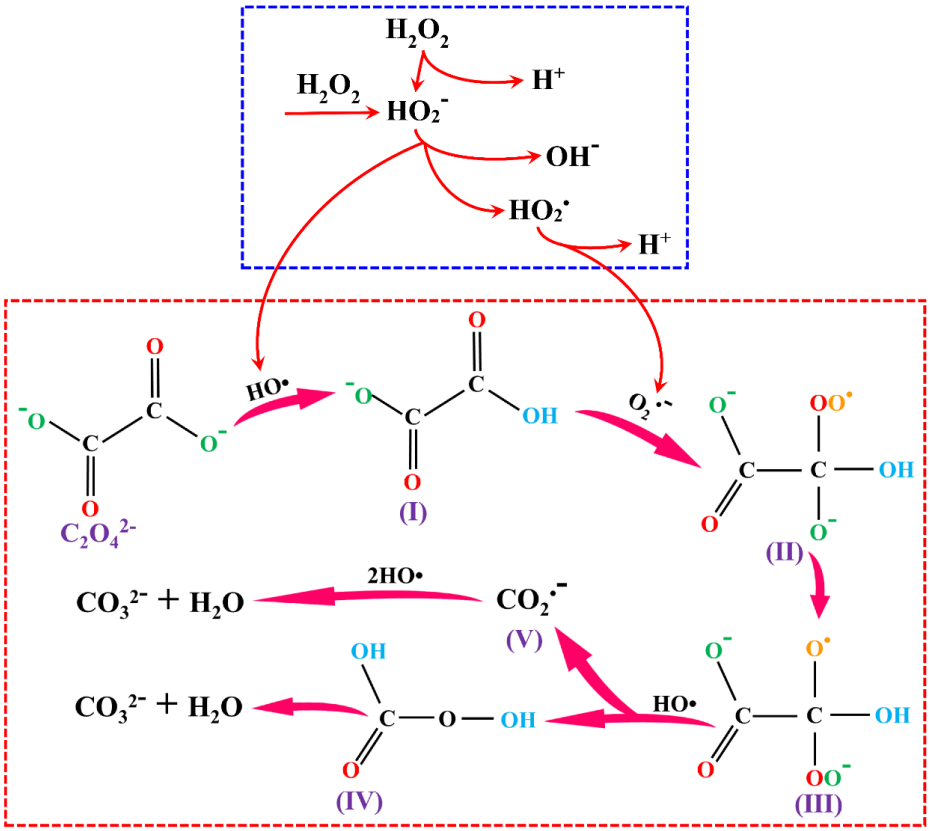

Figure 15. Schematic diagram of $Na_2C_2O_4$ oxidation process.

The XRD analysis results of the filter residue show that the diffraction peaks of the $CaC_2O_4 \cdot H_2O$ and $CaCO_3$ phases are clearly visible in the XRD pattern of the filter residue after oxidation (as depicted in Figure 16). This proved that the organic substance in the leaching solution was indeed oxidized by H_2O_2, while the presence of $CaCO_3$ also confirms the oxidation of $Na_2C_2O_4$.

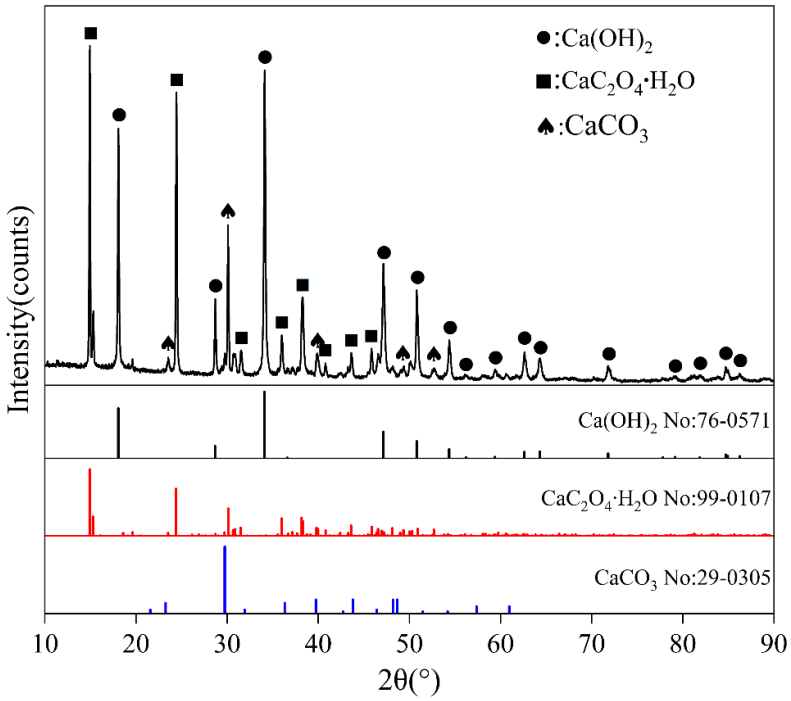

Figure 16. XRD pattern of filter residue after H_2O_2 oxidation-CaO precipitation.

4. Conclusions

(1) Mineralogical studies on bauxite have shown that organic impurities do not form mineral structures in bauxite and their distribution in the ore is not uniform. Organic substances attached to the surfaces of iron minerals and silicon minerals are significantly higher than those on diaspore.

(2) Under the optimal low-temperature ultrasonic-enhanced leaching conditions with ultrasonic power of 550 W, temperature of 80 °C, duration of 60 min, and NaOH concentration of 200 g/L, the TOC leaching rate was 91.02 %, which was 19.01 % higher than conventional leaching. The alumina loss rate was 1.21 %, and the A/S increased from 9.91 to 34.13. The leaching process is jointly controlled by chemical reactions and diffusion, with an activation energy of 34.26 kJ/mol.

(3) AFM detection results of bauxite before and after leaching showed changes in surface protrusions and surface roughness. GC-MS detection results of the leaching solution and oxidation solution revealed the presence of 71 organic substances in the solution.

(4) The H_2O_2 oxidation-CaO precipitation technology is used to purify the leaching solution. H_2O_2 and CaO should be added at 20 % and 800 mL/g, respectively, and then oxidized at temperature of 90 °C with ultrasonic power of 550 W for 60 min. The results indicated that the organic substance was ultimately removed in the form of $CaC_2O_4 \cdot H_2O$ and $CaCO_3$, with a removal rate of 71.35 %. The reaction mechanism of free radicals of organic substances in the alkaline solution of the H_2O_2 oxidation was elucidated.

5. Credit authorship contribution statement

Mengnan Li: Methodology, Data curation, Investigation, Validation, Writing-original draft.
Zhanwei Liu: Conceptualization, Supervision, Project administration, Funding acquisition, Writing-review & editing.
Jiaping Zhao: Writing-review & editing.
Wanzhang Yang: Writing-review & editing.

6. Declaration of Competing Interest

The authors declare that they have no known competing financial interests or personal relationships that could have appeared to influence the work reported in this paper.

7. Data availability

Data will be made available on request.

8. Acknowledgment

We gratefully acknowledge the support received from the National Natural Science Foundation of China (No. 22068021 and No. 52064030), Yunnan Young and Middle-aged Academic and Technical Leaders Reserve Talent Program, China (No. 202305AC160064), Kunming University of Science and Technology Analysis and Testing Foundation (2023P20223102016), Yunnan Major Scientific and Technological Projects (No. 202202AG050011, 202402AB080004 and No. 202202AG050007).

9. References

1. Z. Qu, Y. Liu, Classification and application of chemical alumina, Light Metals, (4) (2015) 20-23.
2. D. Liu, G. Zhang, K. Gui, W. Han, J. Niu, M. Wang, Fabrication of strong and tough alumina ceramic with isotropic textured microstructure at low temperature, J Mater Res Technol 24 (2023) 5159-5164, https://doi.org/ 10.1016/j.jmrt.2023.04. 122.
3. F. Zhu, X. Zhang, X. Guo, X. Yang, S. Xue, Root architectures differentiate the composition of organic carbon in bauxite residue during natural vegetation, Sci. Total. Environ. 883 (2023) 163588, https://doi.org/10.1016/j.scitotenv.2023.16358 8.
4. Z. Wu, H. Lv, M. Xie, L. Li, H. Zhao, F. Liu, Reaction behavior of quartz in gibbsite-boehmite bauxite in Bayer digestion and its effect on caustic consumption and alumina recovery, Ceram. Int. 48 (13) (2022), 18676-18686, https://doi.org/10. 1016/j.ceramint.2022.03.141.
5. G. Power, J.S.C. Loh, C. Vernon, Organic compounds in the processing of lateritic bauxites to alumina Part 2: Effects of organics in the Bayer process, Hydrometallurgy 127 (2012) 125-149, https://doi.org/10.1016/j.hydromet.2012.07. 010.
6. G. Zhou, Y. Wang, T. Qi, Q. Zhou, G. Liu, Z. Peng, X. Li, Toward sustainable green alumina production: A critical review on process discharge reduction from gibbsitic bauxite and large-scale applications of red mud, J. Environ. Chem. Eng. 11 (2) (2023) 109433, https://doi.org/10.1016/j.jece.2023.109433.
7. X. Pan, H. Wu, Z. Lv, H. Yu, G. Tu, Recovery of valuable metals from red mud: A comprehensive review, Sci. Total. Environ. 904 (2023) 166686, https://doi.org/ 10.1016/j.scitotenv.2023.166686.
8. G. Power, J. Loh, Organic compounds in the processing of lateritic bauxites to alumina Part 1: Origins and chemistry of organics in the Bayer process, Hydrometallurgy 105 (1-2) (2010) 1-29, https://doi.org/10.1016/j.hydromet.2010. 07.006.

9. Y. Zhang, R. Xu, H. Tang, L. Wang, W. Sun, A review on approaches for hazardous organics removal from Bayer liquors, J. Hazard. Mater. 397 (2020) 122772, https://doi.org/10.1016/j.jhazmat.2020.122772.
10. F. Busetti, L. Berwick, S. McDonald, A. Heitz, C.A. Joll, J. Loh, G. Power, Physicochemical characterization of organic matter in Bayer liquor, Ind. Eng. Chem. Res. 53 (15) (2014) 6544-6553, https://doi.org/10.1021/ie4028268.
11. Y. Huang, G. Han, J. Liu, W. Wang, A facile disposal of Bayer red mud based on selective flocculation desliming with organic humics, J. Hazard. Mater. 301 (2016) 46-55. https://doi.org/10.1016/j.jhazmat.2015.08.035.
12. T.J. Whelan, A. Ellis, G.S.K. Kannangara, C.P. Marshall, D. Smeulders, M.A. Wilson, Macromolecules in the bayer process, Rev. Chem. Eng. 19 (5) (2003) 431-471, https://doi.org/10.1515/REVCE.2003.19.5.431.
13. H. Yu, B. Zhang, X. Pan, G. Tu, Effect of oxalate on seed precipitation of gibbsite from sodium aluminate solution, J. Cent. South Univ. 27 (3) (2020) 772-779, https://doi.org/10.1007/s11771-020-4330-1.
14. M. Li, Z. Liu, H. Yan, J. Wei, S. Liu, Removal of organic compounds from Bayer liquor by oxidation with sodium nitrate, Hydrometallurgy 215 (2023) 105972, https://doi.org/10.1016/j.hydromet.2022.105972.
15. G. Hefter, A. Tromans, P.M. May, E. Königsberger, Solubility of sodium oxalate in concentrated electrolyte solutions, J. Chem. Eng. Data 63 (3) (2018) 542-552, https://doi.org/10.1021/acs.jced.7b00690.
16. D.E. Smeulders, M.A. Wilson, H. Patney, L. Armstrong, Structure of molecular weight fractions of Bayer humic substances. 2. Pyrolysis behavior of high-temperature products, Ind. Eng. Chem. Res. 39 (10) (2000) 3631-3639, https://doi.org/10.1021/ie000290s.
17. D.W. Laird, C.C. Rowen, T. Machold, P.M. May, G. Hefter, Volatile products from the degradation of organics in a synthetic Bayer liquor, Ind. Eng. Chem. Res. 52 (10) (2013) 3613-3617. https://doi.org/10.1021/ie3024824.
18. B. Zhang, X. Pan, H. Yu, G. Tu, S. Bi, Effect of organic impurity on seed precipitation in sodium aluminate solution, Light Metals, Part F4 (2018) 41-47.
19. J. Wang, Research on removal mechanism of oxalate from sodium aluminate solution [M.Sc. dissertation], Shenyang: Northeastern University (2019).
20. Q. Zhao, X. Zhu, G. Lv, Z. Zhang, Z. Yin, T. Zhang, Calcification transformation of diasporic bauxite, JOM 68 (6) (2016) 1711-1716, https://doi.org/10.1007/s1183 7-016-1930-1.
21. M. Mahmoudian, A. Ghaemi, S. Shahhosseini, Removal of carbonate and oxalate pollutants in the Bayer process using thermal and chemical techniques, Hydrometallurgy 154 (2015) 137-148, https://doi.org/10.1016/j.hydromet.2015.03. 016.
22. M. Xie, F. Liu, H. Zhao, C. Ke, Z. Xu, Mineral phase transformation in coal gangue by high temperature calcination and high-efficiency separation of alumina and silica minerals, J Mater Res Technol 14 (2021) 2281-2288, https://doi.org/10.101 6/j.jmrt.2021.07.129.
23. M.A. Wellington, Effect of thermal treatment of bauxite ore on carbon (organic and inorganic) content and solubility in Bayer process liquor, Ind. Eng. Chem. Res. 52 (4) (2013) 1434-1438, https://doi.org/10.1021/ie3024005.
24. P. Wu, G. Liu, X. Li, Z. Peng, Q. Zhou, T. Qi, Y. Wang, L. Shen, Removal of organics from Bayer liquors via foam flotation, J. Clean. Prod. 336 (2022) 130353, https://doi.org/10.1016/j.jclepro.2021.130353.
25. M. Zarbayani, E. Jorjani, M. Mirmohammadi, M.T. Shadloo, M. Noaparast, Mineralogical and sink-float studies of Jajarm low-grade bauxite, Int J Min Met Mater 17 (3) (2010) 251-256, https://doi.org/10.1007/s12613-010-0301-0.
26. S. Fan, W. Chen, G. Liang, Behavior of sodium oxalate in seeded precipitation process of sodium aluminate solution, Chinese J Eng 40 (1) (2018) 51-58, https://doi.org/10.13374/j.issn2095-9389.2018.01.007.

27. B. Zhang, X. Pan, J. Wang, H. Yu, G. Tu, Reaction kinetics and mechanism of calcium oxide in dilute sodium aluminate solution with oxalate based on lime causticization, T NONFERR METAL SOC 29 (6) (2019) 1312-1322, https://doi.org/10.1016/S1003-6326(19)65038-7.
28. M. Xie, H. Lv, H. An, F. Liu, H. Zhao, Effect of alkali doping on the preparation of calcium aluminate by aluminium dross calcification process, Environ. Technol. Innovation 32 (2023) 103312, https://doi.org/10.1016/j.eti.2023.103312.
29. G. Liu, W. Dong, T. Qi, Q. Zhou, Z. Peng, X. Li, Behavior of calcium oxalate in sodium aluminate solutions, T NONFERR METAL SOC 27 (8) (2017) 1878-1887, https://doi.org/1887. 10.1016/S1003-6326(17)60212-7.
30. Z. Liu, M. Mohseni, S. Sauvé, B. Barbeau, Segmented regeneration of ion exchange resins used for natural organic matter removal, Sep. Purif. Technol. 303 (2022) 122271, https://doi.org/122271. 10.1016/j.seppur.2022.122271.
31. Sentana, M.A. De La Rubia, M. Rodríguez, E. Sentana, D. Prats, Removal of natural organic matter by cationic and anionic polyacrylonitrile membranes. The effect of pressure, ionic strength and Ph, Sep. Purif. Technol. 68 (3) (2009) 305-311, https://doi.org/10.1016/j.seppur.2009.05.017.
32. P. Wu, G. Liu, X. Li, Z. Peng, Q. Zhou, T. Qi, Effects of CMC and micelle formation on the removal of sodium benzoate or sodium stearate in a sodium aluminate solution, JOM 72 (1) (2020) 263-269, https://doi.org/10.1007/s11837-019-03853-6.
33. S. Marciano, N. Mugnier, P. Clerin, B. Cristol, P. Moulin, Nanofiltration of Bayer process solutions, J. Membr. Sci. 281 (2006) 260-267, https://doi.org/10.101 6/j.memsci.2006.03.040.
34. U. Baig, A. Waheed, I.H. Aljundi, R.A. AbuMousa, Facile fabrication of graphitic carbon nitride nanosheets and its integrated polyamide hyper-cross-linked TFC nanofiltration membrane with intrinsic molecular porosity for salts and organic pollutant rejection from water, J Mater Res Technol 15 (2021) 6319-6328, https://doi.org/10.1016/j.jmrt.2021.11.027.
35. M.A.S Pastor, A.B.B. Junior, D.C.R. Espinosa, J.A.S. Tenório, M.D.P.G. Baltazar, Application of advanced oxidation process using ozonation assisted with hydrogen peroxide for organic compounds removal from bayer liquor, Ozone Sci Eng 44 (3) (2022) 291-301. https://doi.org/10.1080/01919512.2021.1924118.
36. H. Wang, B. Quan, G. Bo, Y. Zhang, L. Liu, J. Zhang, X. Zhang, C. Zhang, Advanced oxidation treatment of dissolved organic matter from wastewater treatment plant secondary effluent using scattering electrical reactor, J. Clean. Prod. 267 (2020) 122258, https://doi.org/10.1016/j.jclepro.2020.122258.
37. J. Qiu, Z. Chen, K. You, H. Luo, Enhanced removal of heavy metal from stainless steel pickling sludge by sonochemical cavitation: Physical fragmentation and chemical activation, J. Environ. Chem. Eng. 12 (2) (2024) 111983, https://doi.org/10.1016/j.jece.2024.111983.
38. Q. Gui, L. Fu, Y. Hu, H. Di, M. Liang, S. Wang, L. Zhang, Gold extraction using alternatives to cyanide: Ultrasonic reinforcement and its leaching kinetics, Miner. Eng. 191 (2023) 107939, https://doi.org/10.1016/j.mineng.2022.107939.
39. T. Nshizirungu, M. Rana, Y.T. Jo, E. Uwiragiye, J. Kim, J.H. Park, Ultrasound-assisted sustainable recycling of valuable metals from spent Li-ion batteries via optimisation using response surface methodology, J. Environ. Chem. Eng. 12 (2) (2024), 112371, https://doi.org/10.1016/j.jece.2024.112371.
40. J. Liu, S. Wang, C. Liu, L. Zhang, D. Kong, Mechanism and kinetics of synergistic decopperization from copper anode slime by ultrasound and ozone, J. Clean. Prod. 322 (2021) 129058, https://doi.org/10.1016/j.jclepro.2021.129058.
41. F. Zheng, H. Zhu, T. Luo, H. Wang, H. Hou, Pure water leaching soluble manganese from electrolytic manganese residue: Leaching kinetics model analysis and characterization, J. Environ. Chem. Eng. 8 (4) (2020) 103916, https://doi.org/10.1016/j.jece.2020.103916.

42. Y. Wan, C. Xin, W. Ding, H. Zhang, H. Yang, S. Bao, Kinetics and mechanism of ultrasonic-enhanced mixed acid leaching of zinc from zinc-bearing dust, J. Environ. Chem. Eng. (2024) 113246, https://doi.org/10.1016/j.jece.2024.113246.
43. M.A.S. Pastor, A.B.B. Junior, J.A.S. Tenório, D.C.R. Espinosa, M.D.P.G. Baltazar, Use of O_3 and O_3/H_2O_2 for degradation of organic matter from Bayer liquor towards new resource management: Kinetic and mechanism, Can J Chem Eng. 101 (4) (2023) 2094-2103, https://doi.org/10.1002/cjce.24605.